Master Advanced Lab Course
Universität Göttingen – Fakultät für Physik

Report on
the experiment KT.HIP

Higgs physics with the ATLAS experiment

Name: Eric Bertok

Email: eric.bertok@stud.uni-goettingen.de

Conducted on   19th April 2018

Assistant: K. Abeling

Copy of document requested: ☐ yes   ☑ no

Unterschrift:

Submission

Date: Signature of assistant:

Review

Date: Name of examiner:

Points: Signature:

Mark:

Contents

1 Introduction

2 Theory

2.1 A summary of the Standard Model

The Standard Model (SM) is the combination of different theories governing three of the four known fundamental forces (electromagnetic, weak and strong interactions), as well as all known elementary particles and their interaction. It consists of 6 quarks making up the hadrons, 6 leptons, as well as 4 gauge bosons acting as force carriers for the interaction between the other particles. The interactions are fixed by the principle of local gauge invariance. The last puzzle piece - the Higgs boson - has recently been found at the LHC. It gives mass to the other particles by the Higgs mechanism, a form of spontaneous symmetry breaking. The Standard model has been a great success, having made predictions for new physics as well as confirming these predictions with great accuracy. An example of this is the theory of quantum-electro-dynamics, which has been confirmed to an astounding precision [cite]. Despite the great success, the Standard Model is a rather ad-hoc combination of different ideas without a unifying underlying theoretical principle. It features 26 free parameters, namely the fermion masses, the coupling strengths of the fundamental forces, mixing angles of quarks and neutrinos and parameters specifying the Higgs mechanism [5, p. 500]. Therefore, it is desired that all four forces would unify into a "Great Unified Theory" (GUT). There are other obvious shortcommings of the SM: Gravity is not part of the SM, meaning that general relativity is not compatible with it, although being much weaker than the other forces, it can be neglected in particle experiments. Furthermore, dark matter is not described by the SM. Furthermore, the mass of the Higgs boson does not have the right mass order of magnitude at very high energy scales due to loop corrections, a problem known as the "hierarchy problem" [5, p. 505].

2.2 Beyond the Standard Model

Several ideas exist for an extension of the SM. Supersymmetry is an attempt to both unify the electroweak and strong force as well as solving the hierarchy problem. In supersymmetry, every elementary particle would have a corresponding super-partner, called a "sparticle". So far, no super-partners have been found [5]. Also, there would be the need for 5 different Higgs bosons. There is also a possibility of extra space-like dimensions that are hidden from us, which would be a possible explanation for the weakness of gravity. A prominent theory of quantum gravity - string theory - predicts these extra dimensions. In an experiment, these extra dimensions could manifest as a large amount of missing energy [6]. Additionally, neutrino masses need to be explained. A prominent idea is that neutrinos are majorana particles, namely particles being their own antiparticles.

2.3 The Higgs mechanism

[5, Ch. 17] The Higgs mechanism is needed in the SM to give rise to massive gauge bosons and fermions in a locally gauge invariant manner. The problem can be illustrated with a simplified toy model. Consider a mass term for a vector boson (e.g. a photon) in the Lagrangian:

$$\mathcal{L}_{\text{mass}} = \frac{1}{2} m_\gamma A_\mu A^\mu. \tag{2.1}$$

Such a term is not invariant under a local gauge transformation

$$\partial_\mu \rightarrow D_\mu = \partial_\mu + ig A_\mu \tag{2.2}$$
$$A_\mu \rightarrow A'_\mu = A_\mu - \partial_\mu \chi(x). \tag{2.3}$$

One now introduces a complex scalar field $\phi(x)$ with a mexican hat potential $V(\phi) = \mu^2 \phi^2 + \lambda \phi^4$, which is shown in fig. 1. For $\mu^2 < 0, \lambda > 0$, the potential minimum shifts from the origin at $\phi = 0$ to a degenerate ring in the complex plane. The ground state thus chooses a new vacuum in an arbitrary direction with nonzero ϕ, a process called "spontaneous symmetry breaking". This ground state can now be expanded around this minimum, choosing a convenient gauge, to describe the system's low energy excitations in this new vacuum. This gives rise to a massless particle called the Goldstone boson, as well a massive scalar particle, called the Higgs boson. The original lagrangian expressed in this gauge around this new minimum now has a mass term for the vector bosons without having broken local gauge invariance. The standard model Higgs has more subtleties arising from the noncommutativity of the SU(2) and SU(3) gauge symmetries, but the general principle stays the same.
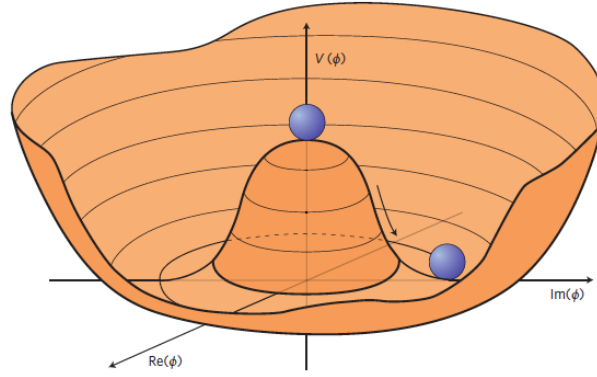
Figure 1: The mexican hat potential for the scalar Higgs boson. The symmetric state at $\phi = 0$ is spontaneously broken and a new vacuum state is chosen in a random direction. For a particular choice of ground state, the low-energy excitations look like a massive scalar field in addition to a massless Goldstone field. After a local gauge transformation, a mass term for the vector bosons becomes visible in the lagrangian [3].

2.4 Higgs decay and production

Apart from maybe neutrinos, whose mass-genertating principle is not yet known, the Higgs boson couples and thus can decay to all SM particles. However, the top quark is too massive to be a real decay product of the Higgs boson. Since the Higgs couples proportionally to the mass of the particle, decays to heavier particles are favoured. The largest decay channels are to bottom quarks (57.8%), W bosons (21.6%) and tau leptons (6,4%). Even though photons are massless, they can be the result of a Higgs decay by means of virtual top quark loops. The Branching ratio to photons is only 0.2%. At the LHC, the two most important Higgs production mechanisms are gluon-gluon fusion and vector boson fusion [5, p. 490f]. Although the former has a significantly higher cross section ($10\times$ higher), vector boson fusion is more practical, since the virtual top quark loops lead to QCD radiation from the colour field that makes identifying a Higgs decay more challenging.

Since Higgs decays are hard to seperate from the usual multi jet events at the LHC, decay channels with distinctive final state topologies are favoured. These include $H \rightarrow \gamma\gamma$ and $H \rightarrow ZZ^* \rightarrow l^+l^-l^+l^-$. In this lab, the four lepton states are the most important. These have to be seperated from other four lepton state processes such as $t\bar{t}$ pair production, where each of the two top quarks sends out two W bosons, changing flavour each time. These W's can then each decay into a lepton neutrino pair. Another background four-lepton process is the combination of a Z decaying into two leptons together with a $b\bar{b}$ pair, each decaying into a lepton, neutrino pair via a W boson.

3 Experimental setup and methods

3.1 ATLAS detector

The ATLAS detector is one of four major experiments at the Large Hadron Collider at Cern. It is build for general purpose experiments with propton-proton collisions. Its main goal has been the detection of the Higgs boson, tests of the Standard Model and search for new physics beyond the SM, such as supersymmetry and extra dimensions. The detector itself consists of a inner detector, a calorimeter and the muon spectrometer. The inner detector is a collection of different systems like a pixel detector and semiconductor tracker for measuring the direction, momentum and charge of charged particles, which are brought on a circular path by large magnetic fields parallel to the beam axis. The transition radiation tracker additionally provides information on which type of particle was detected. Next, the electromagnetic and hadronic calorimeters are designed to absorb as much energy of the produced particles as possble. This yields the direction and energy of particles as well as a means to distinguish leptons from hadrons. Muons however, being a weakly ionising particle mostly flies through these calorimeters. Therefore, the largest part of the detector is the muon spectrometer, which is there to give very precise measurements of the muon momentum. The parameters that are used to describe particle trajectories and energy-momentum are

- The azimuthal angle ϕ

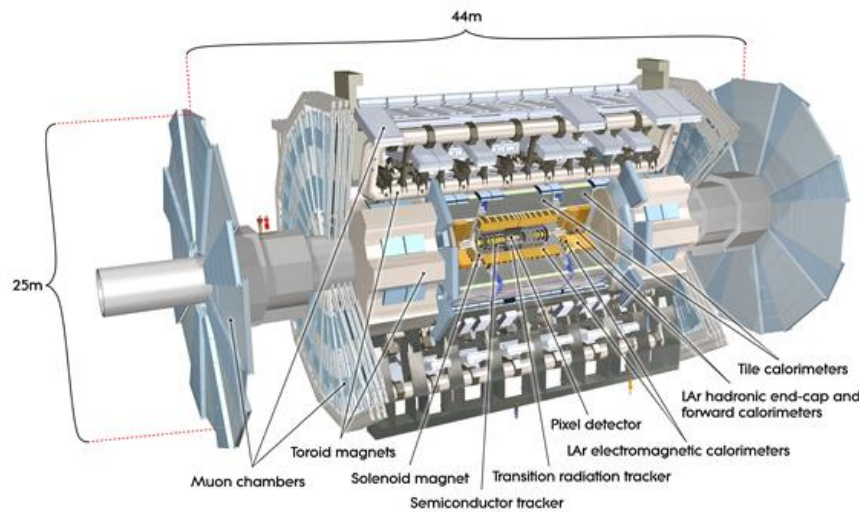- The pseudorapidity $\eta = -\ln\left[\tan\left(\frac{\theta}{2}\right)\right]$

Figure 2: Cross section of the ATLAS detector [2]

- the z coordinate along the beam axis

- the transverse momentum $p_T = \sqrt{p_x^2 + p_y^2}$

3.2 trigger?

3.3 ATLAS event display

ATLANTIS, the ATLAS event desplay is used to depict the detector responses for various decay processes graphically to get a feel for the different decay topologies. From a view along the z-axis aswell as from a side view, the tracks in the inner detector and the muon spectrometer, as well as the showers in both calorimeters can be seen. Additional information on the measured quantities can be obtained upon selection of these features.

3.4 Signifikanz????

[1]

4   Analysis

4.1 Detector Responses to specific processes

For this part of the lab, simulated data for single particle detection are evaluated using ATLANTIS. Of course, such a single particle process is highly unphysical because of background and additional decay products.

Electron, e^-

For a single electron, a well-defined single track in the inner detector is observed. Its curvature is due to the electric charge and the magnets which force the particle on a curved trajectory. Aligning with the track is a small deposit in the electronagnetic calorimeter right behind the inner detector. There, electrons radiate photons that lead to electron-positron pair production. This leads to a shower.
In rare cases, the tracks in the inner detector are not consistent with the showers in the calorimeter. Therefore it is clear that reconstruction errors are still possible in such simple cases. There is also a possibility that an electron emits a photon before reaching the calorimeter.
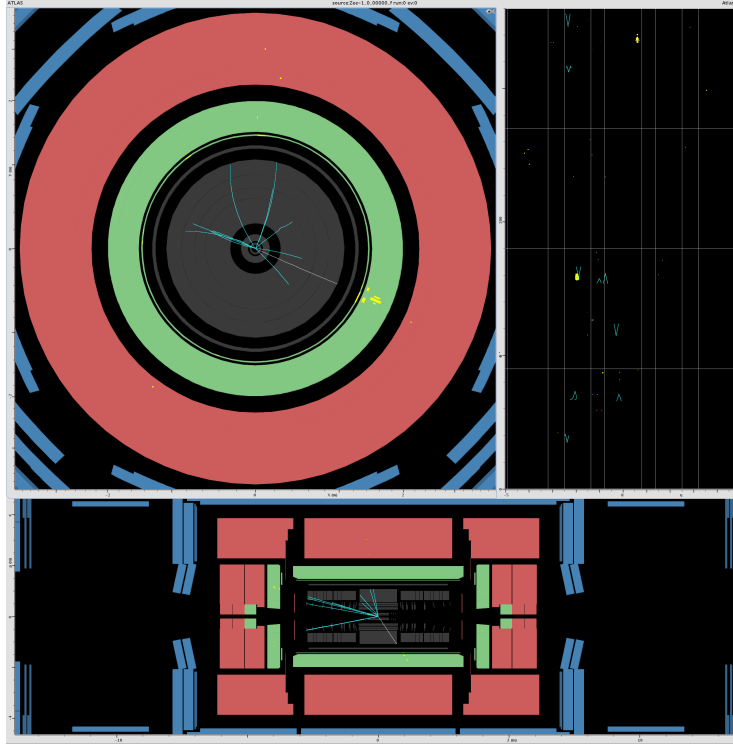
Figure 3: Z$\to e^+e^-$ decay viewed in ATLANTIS

Muon, μ^-

Muons are especially easy to identify by a long track in the muon spectrometer that is consistent with a track in the inner detector. As they have a mass of around 100 GeV, they are minimally ionising, meaning that they pass through both calorimeters with virtually no trace. This is the reason for the large muon spectrometers in the first place.

Photon, γ

Photons leave mostly no tracks inside the spectrometers since they are electrically neutral and don't typically ionize. However, there is the possibility of electromagnetic radiation leaving ionization tracks in the inner detector which leads to a possible misidentification as electrons. The calorimeter responses are equivalent to those of an electron.

Tau, τ

Proper identification of tau leptons is very tricky as it is not directly observable owing to its very short lifetime. Only its decay products are visible in the detector. It decays via the weak interaction, always producing at least one tau-neutrino in addition to mostly either an electron-neutrino or muon-neutrino pair, or a pion. The latter subsequently decay mostly into $\mu\nu_\mu$ pairs in the case for charge pions or two photons in the case of neutral pions. Reconstructing taus is therefore very challenging, due to the plethora of possible decay products, as well as the neutrinos, which are invisible to the detector and have to be inferred from indirect measurements of the missing transverse momentum. The observed tau events are often similar to either the electron or muon case. But also different topologies are possible, e.g. three tracks and small deposits in the hadronic calorimeter in addition to deposits in the electromagnetic calorimeter. Rarely, a muon track is observed in the muon spectrometer owing to the decay of a neutral pion.

Dijets

The dijet events consist of a large amount of tracks and energy deposits. The strong force does not allow for the free propagation of single quarks or gluons. Instead, quarks and gluons hadronise creating additional quark pairs and gluons. This results in cone shaped tracks and deposits in the calorimeters. These hadron showers -also referred to as jets- are typical in proton proton collisions and form a large part of the background. Typically two jets will stand out from the rest in their high energy, leaving the biggest deposit in the calorimeters. Aditionally, they are minimally

Event	Inner Detector		Muon Spectrometer		Loss	
	p_{ID} [GeV]	$p_{T,ID}$ [GeV]	p_{MS} [GeV]	$p_{T,MS}$ [GeV]	Δp [GeV]	Δp_T [GeV]
1	−85.28	−38.36 ± 1.016	−57.62	−25.72	27.66	12.64 ± 1.016
2	43.40	33.17 ± 0.797	47.53	36.17	−4.13	−3.00 ± 0.797
3	−241.37	−41.85 ± 3.633	−240.72	−41.67	0.65	0.18 ± 3.633
4	48.89	41.96 ± 0.831	−48.47	41.26	0.42	0.70 ± 0.831
5	−168.16	−53.66 ± 2.054	−181.32	−62.44	−13.6	−8.78 ± 2.054
6	117.32	44.65 ± 1.388	100.26	38.01	17.06	6.64 ± 1.388
7	−71.94	−57.39 ± 1.684	−68.66	−54.77	3.28	2.62 ± 1.684
8	199.91	64.54 ± 2.677	203.14	66.99	−3.23	−2.45 ± 2.677
9	−57.84	−55.54 ± 1.150	−53.71	−51.16	4.13	4.38 ± 1.150
10	−100.75	−37.79 ± 1.185	−97.81	−36.40	2.94	1.39 ± 1.185
11	38.26	37.59 ± 0.653	38.18	37.48	0.08	0.11 ± 0.653
12	−105.19	−59.88 ± 1.766	−112.38	−64.27	−7.19	−4.39 ± 1.766
13	236.12	47.52 ± 3.324	267.31	53.73	−31.19	−6.21 ± 3.324
14	−131.69	−43.88 ± 1.471	−129.21	−43.21	2.48	0.67 ± 1.471
15	152.24	45.66 ± 1.844	161.39	48.37	−9.15	−2.71 ± 1.844
16	−35.23	−33.65 ± 0.539	−35.88	−33.23	−0.65	0.42 ± 0.539
17	54.19	52.80 ± 1.060	53.70	52.33	0.49	0.47 ± 1.060
18	−84.75	−64.49 ± 2.515	−71.79	−55.02	12.96	9.47 ± 2.515
19	104.26	47.56 ± 1.324	111.68	51.21	−7,42	−3.65 ± 1.324
20	−184.01	−35.52 ± 2.24	−174.36	−33.96	9.65	1.56 ± 2.284

Table 1: Momenta p, and transverse momenta p_T for the first twenty events, measured both in the inner detector and the muon spectrometer. The difference between these p_{loss}, $p_{T\,\text{loss}}$ is also shown. Negative losses indicate a gain in momentum after passing the calorimeters.

curved in the inner detector due to their large momentum. These two jets are therefore identified as coming directly from the interactions of the partons making up the original protons that collided. The rest of the jets originate from low energy charged particles.

4.2 Analysis of muon momenutm loss

For the single muon dataset, both the momentum p and the transverse momentum p_T are read out using ATLANTIS for the first 20 events. Values are read out from the inner detector (ID) and the muon spectrometer (MS). An uncertainty σ is also given for both values for the inner detector. Contrary to the multi purpose inner detector, the uncertainty is assumed to be negligible for the muon spectrometer, since its size allows for large tracks and therefore great accuracy. Additionally the muon detector elements are specialized for muons. The loss of (transverse) momentum $\Delta p_{(T)} = |p_{(T)\text{ID}}| - |p_{(T)\text{MS}}|$ is calculated. Uncertainty is propagated using the gaussian formula. The result is shown in table 1. Interestingly, for 7 out of the 20 events, the muon spectrometer measured a higher transverse momentum than the inner detector. This is furthermore not consistent with the uncertainties from the inner detector. [???]

The average loss of momentum is calculated with a weighted average:

$$\bar{p} = (\sum \frac{p}{\sigma^2})/(\sum \frac{1}{\sigma^2}), \qquad \sigma_{\bar{p}} = \sqrt{1/(\sum \frac{1}{\sigma^2})}. \tag{4.1}$$

One obtains

$$\bar{\Delta} p_T = (0.91 \pm 0.25) \text{ GeV}. \tag{4.2}$$

In the assumption that negative momentum losses are unphysical and thus ignoring them, one obtains instead:

$$\bar{\Delta} p_T = (2.12 \pm 0.28) \text{ GeV}. \tag{4.3}$$

4.3 Reconstruction of the Z mass

Simulated data from $Z \to e^+ e^-$ events are analyzed using ATLANTIS. Here, events with two distinct high energy deposits in the calorimeter could be found. These are assumed to be the electron and positron respectively. An

		Inner Detector				EM Calorimeter	
		ϕ	η	p_T [GeV]	p [GeV]	E [GeV]	E_T [GeV]
a)	e_1	5.860	0.610 ± 0.001	-19.20 ± 0.297	-22.88	22.2	18.6
	e_2	2.771	-1.953 ± 0.001	25.38 ± 0.860	91.29	88.6	24.6
b)	e_1	5.187	2.193 ± 0.000	-44.75 ± 2.673	-202.97	175.4	38.6
	e_2	1.485	2.432 ± 0.002	3.72 ± 0.180	21.84	259	45.5
c)	e_1	0.826	-0.610 ± 0.001	-41.69 ± 0.752	49.69	49.9	42.0
	e_2	3.926	-0.983 ± 0.001	39.98 ± 1.581	60.92	58.0	38.4

Table 2: ATLAS Parameters for both leptons in three $Z \to e^+ e^-$ events.

	M_Z [GeV] from ID	M_Z [GeV] from EM Cal.
a)	85.7 ± 1.6	83.2 ± 0.1
b)	28.8 ± 1.0	71.8 ± 0.1
c)	83.1 ± 1.9	80.0 ± 0.1

Table 3: Reconstructed Z boson mass, M_Z, from three $Z \to e^+ e^-$ events with the transverse energy obtained from either the inner detector or the EM calorimeter.

example of such an event is seen in fig. 3. By selecting the tracks or the calorimeter deposits manually, various parameters can be read off. For the tracks in the inner detector, the azimuthal angle ϕ, the pseudorapidity η and both the transverse and total momentum $P_{(T)}$ were noted. From the electromagnetic calorimeter the total and transverse energy $E_{(T)}$ was taken. The values are summed up in table 2.

The invariant mass of the Z boson can be written as the four-vector norm-squared of the sum of the energy momentum vectors of both leptons:

$$M_Z^2 = (p_1^\mu + p_2^\mu)^2 = m_1^2 + m_2^2 + 2[E_1 E_2 - \vec{p_1} \cdot \vec{p_2}] \tag{4.4}$$

$$= m_1^2 + m_2^2 + 2[E_1 E_2 - (E_{T_1} E_{T_2}(\beta_{T_1} \beta_{T_2} \cos(\Delta\phi) + \sinh(y_1)\sinh(y_2)))]. \tag{4.5}$$

In the second line, the three-vector scalar product has been expanded in terms of the rapidity y, the azimuthal angle ϕ and the transverse (rel.) velocity β_T. For a highly relativistic electron with $p = 50$ GeV, the rest mass can be ignored, thus setting $m_1 = m_2 = 0$, $E_{(T)} = p_{(T)}$, $\beta_{(T)} = 1$, $\eta = y$, which reduces the Z mass formula to

$$M_Z = \sqrt{2 E_{T_1} E_{T_2} (\cosh(\Delta y) - cos(\Delta\phi))}. \tag{4.6}$$

Errors are calculated by the usual gaussian error propagation. However, it has to be kept in mind that the only uncertainty given by the detector was that of the transverse momentum measured in the inner detector and the pseudorapidity. A large amount of uncertainty can also be attributed to the selection of the energy deposits in the calorimeter, which was done manually. However such an error has not been included. The final results are shown in table 3. Clearly, for event b), the result does not conform to the literature value and the total momentum of the second lepton does not have the same order of magnitude as the calorimeter energy.

4.4   Determination of cut criteria for ZZ selection

The aim of this part of the lab is the development of cut criteria to extract the signal of $ZZ \to llll$ processes from the background of the $t\bar{t}$ pair production and the $Zb\bar{b}$ background summarized in section 2.4. The datasets used are all monte-carlo simulations. The Z^0 pair signal corresponds to an integrated luminosity of 400 fb^{-1}, while all other datasets correspond to 140 fb^{-1}. Different event parameter distributions are plotted for both signal and background to determine which parameters have a large amount of signal events and a small amount of background events, or vice-versa. Because all background processes lead to additional quarks produced with the four leptons, the jet properties of the events is used to extract the signal. First, the number of jets per event is shown in fig. 4. As expected, the background processes have a larger number of jets. Thus, a cut requiring

$$n_{\text{jets}} \leq 2 \tag{4.7}$$

is chosen. Furthermore, since the quarks are produced alongside the leptons, a larger amount of energy deposit noise around the leptons is expected. figs. 5 and 6 show this calorimeter noise et_{iso} around both the most and least

energetic lepton. For the intermediate leptons, the plots look similar. Background processes have a larger amount of noise, leading to the cut condition

$$et_{iso} \leq 5 \text{ GeV}. \tag{4.8}$$

Additional parameters such as the missing transverse energy were probed but did not lead to a better reconstruction of the signal. The amount of signal and background events before and after the cuts are summarized in 4.
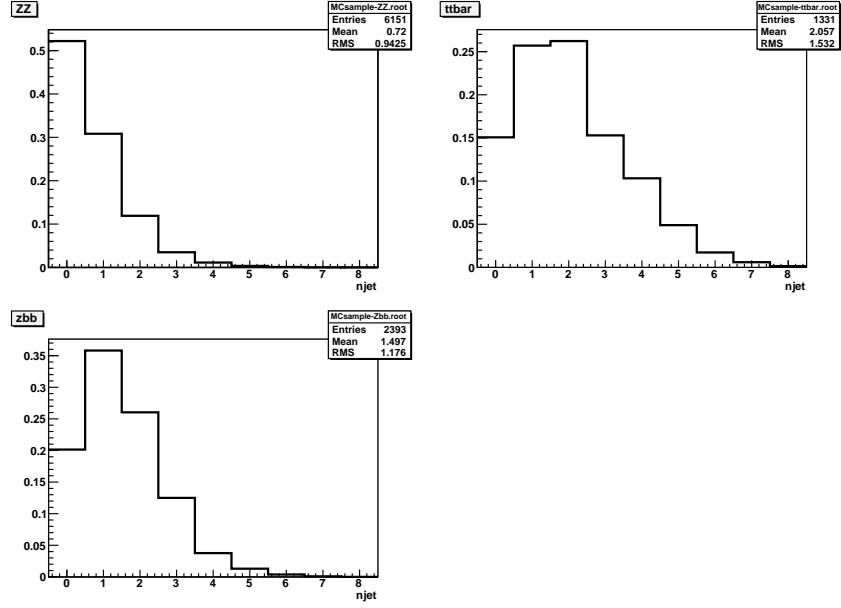

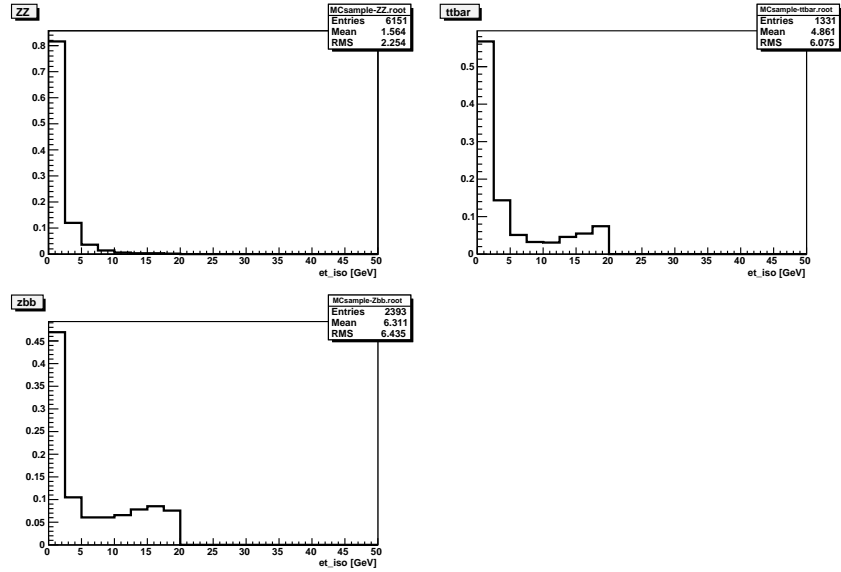Figure 4: Number of jets for the ZZ signal and the $t\bar{t}$ and Zbb monte carlo data.

Figure 5: Calorimeter energy deposit around the most energetic lepton for the ZZ signal and the $t\bar{t}$ and Zbb monte carlo data.
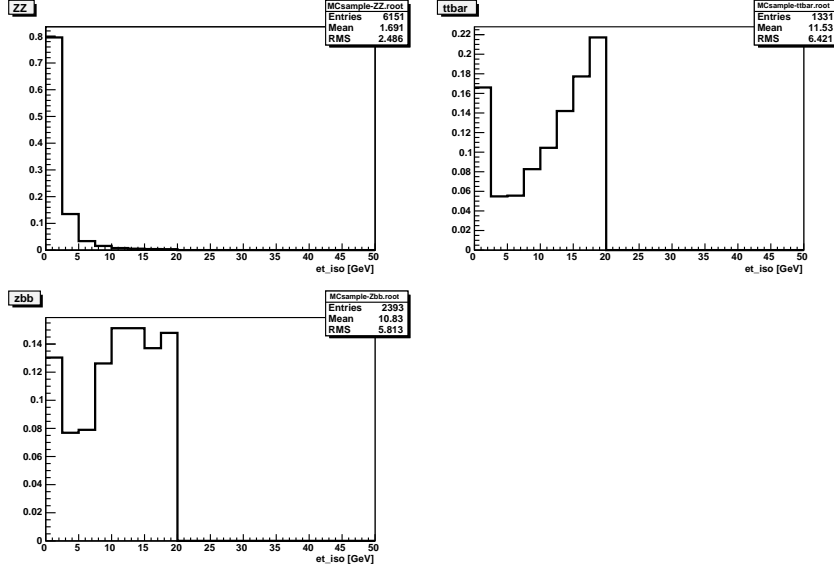
7

Figure 6: Calorimeter energy deposit around the least energetic lepton for the ZZ signal and the $t\bar{t}$ and Zbb monte carlo data.

Process	Events before cut	Events after cut
ZZ (sig)	6151	4561
Zbb (bkg)	2393	17
$t\bar{t}$ (bkg)	1331	0

Table 4: Number of events before and after application of the cut criteria detailed above on the signal and background processes.

4.5 Mystery ZZ production threshhold

With the cuts above in place, a simulated "mystery" data set with an integrated luminosity of 100 fbî$^{-1}$is investigated with respect to ZZ pairs. A Z boson is defined as a real one, if its mass is within two decay withs $2\Gamma_Z = 4.99$ GeV around the nominal Z mass $m_Z = 91.19$ [4]. It can now be counted, whether the two Z bosons produced are both real (ZZ), both virtual (Z^*Z^*) or mixed (ZZ^*). To ensure that the two leptons belonging to a particular Z boson are identified correctly, only the datasets with 2 electrons and 2 muons are used. If the invariant mass of all four leptons is greater or equal to twice the Z mass, the threshold is reached. This can be seen from

$$M_{4l} = (\sum_{i=1}^{4} p_i^{\mu})^2 = (p_1^{\mu} + p_2^{\mu})^2 + (p_3^{\mu} + p_4^{\mu})^2 + 2(p_1^{\mu} + p_2^{\mu})(p_{3,\mu} + p_{4,\mu}) \tag{4.9}$$

$$= 2M_Z + 2(p_1^{\mu} + p_2^{\mu})(p_{3,\mu} + p_{4,\mu}) \geq 2M_Z, \tag{4.10}$$

with lepton 1 and 2 originating from one Z and 3 and 4 originating from the other. The counting results are summed up in table 5.

	Above Threshold	Below Threshold
ZZ	934	13
ZZ^*	1553	319
Z^*Z^*	476	162

Table 5: Number of events above and below the production threshold, on-shell (ZZ), off-shell (Z^*Z^*), and mixed (ZZ^*) discovered in the provided mystery datasets.

4.6 Higgs Boson and New Physics

Here, three "mystery" data sets containing new physics and a simulated standard model ATLAS data set are analyzed. First, new physics is searched in the mystery data. Several variable distribution were plotted against another to find differences in the four data sets. After trying out various variables, it was found that a selection of

- Missing transverse energy $etmis \geq 100$ GeV

- Calorimeter noise around each lepton $et_{iso} \leq 10$ GeV

left around 10% of the events in mystery data set 2, while all other data sets saw a reduction in events to 1% (ATLAS) and 3% (mystery 3 and 4) of the initial events. The cut variable distribution are shown in figs. 7 to 9, while the final invariant mass distribution after the cuts are shown in fig. 10.
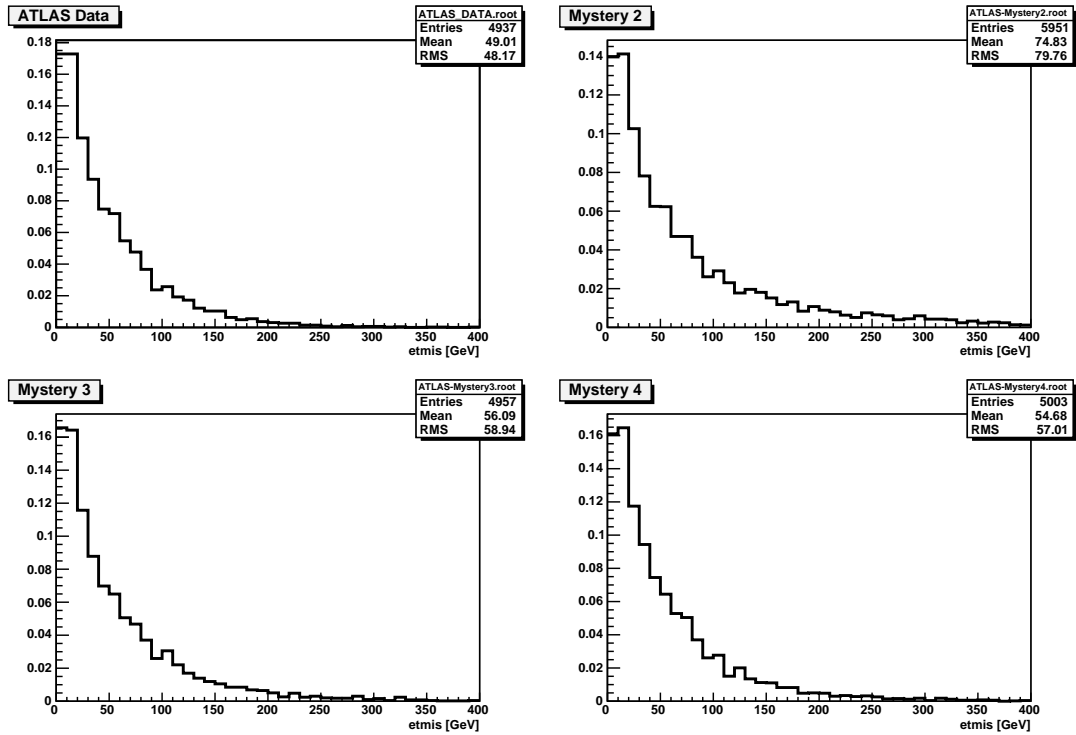

Figure 7: Missing transverse energy distribution of the simulated ATLAS data and three mystery data sets.

Defining the mystery data set 2 as the signal, the significance is calculated with [1]

$$Sig = \frac{S}{\sqrt{S+B}}, \tag{4.11}$$

where S and B are the number of events in the signal and background respectively, while the initial uncertainty is calculated with a poisson error $\sigma_S = \sqrt{S}, \sigma_B = \sqrt{B}$. Thus, eq. (4.11) gives a measure of the sensitivity that the signal is measured on top of the fluctuations of the signal and background. The amount of signal events S are calculated by scaling the signal dataset to the luminosity of the ATLAS data of 149 fb^{-1} and then subtracting the ATLAS data???

5 Discussion

References

[1] http://www.pp.rhul.ac.uk/~cowan/atlas/cowan_statforum_8may12.pdf.   – Zugriff:2018-04-23

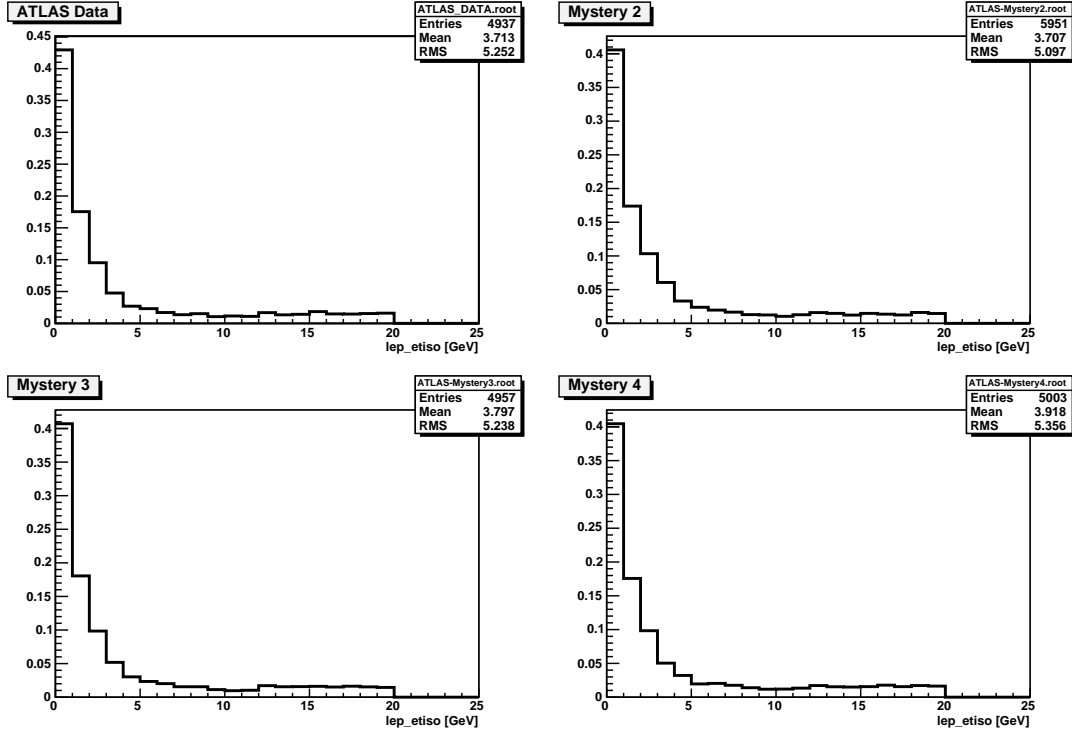Figure 8: Calorimeter noise distribution for the most energetic lepton of the simulated ATLAS data and three mystery
data sets.

[2] : *Cern, ATLAS detector*. https://atlas.cern/discover/detector

[3] *Cern website*. `https://cds.cern.ch/record/2012465/files/higgspotential.png`. –
Zugriff:2018-04-23

[4] *Partlicle Data Group: gauge boson summary sheet*. `http://pdg.lbl.gov/2017/tables/`
`rpp2017-sum-gauge-higgs-bosons.pdf`. – Zugriff:2018-01-31

[5] THOMSON, Mark: *Modern Particle Physics*. Cambridge University Press, 2013

[6] ZWIEBACH, Barton: *A first course in string theory*. Cambridge university press, 2004
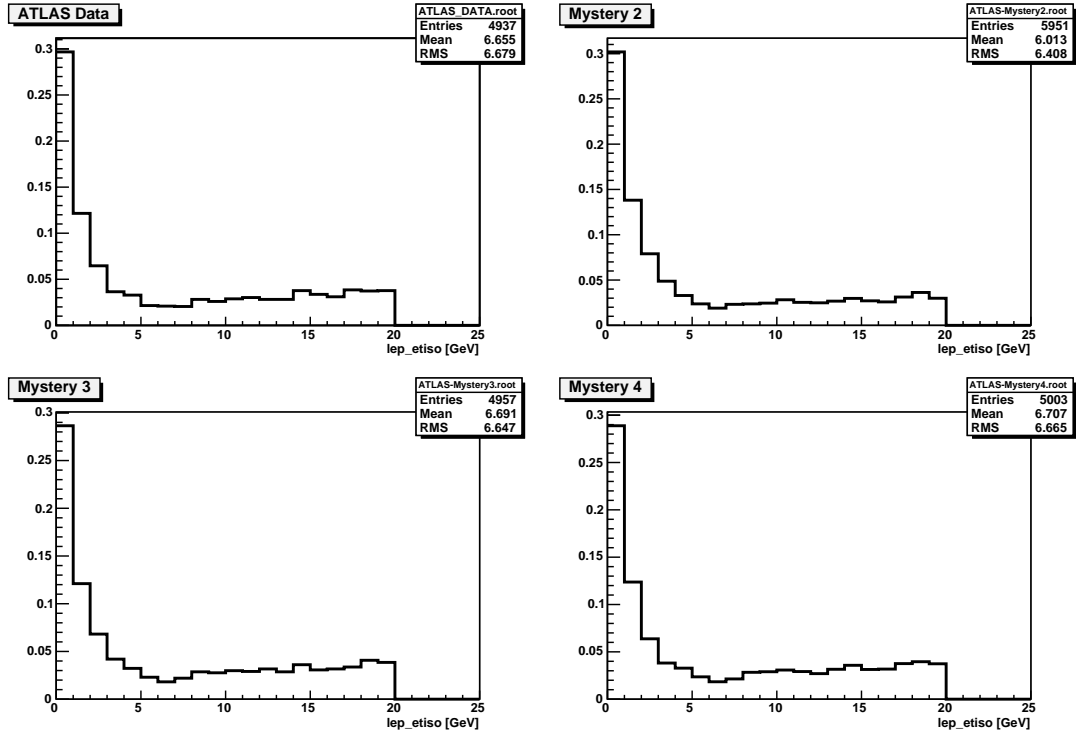
Figure 9: Calorimeter noise distribution for the least energetic lepton of the simulated ATLAS data and three mystery data sets.
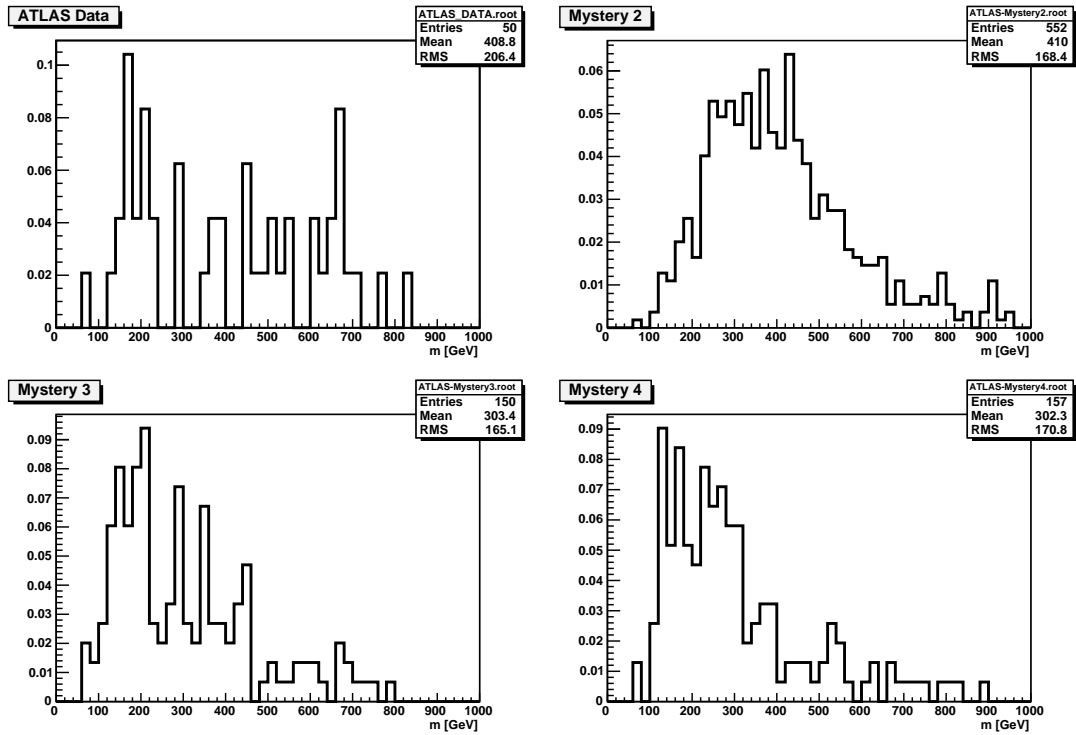

Figure 10: Invariant mass distribution of the four leptons of the simulated ATLAS data and three mystery data sets.

11